Macromolecules
ARTICLE

Macromolecules **2009**, *42*, 5983–5995 **5983**
DOI: 10.1021/ma9003506

Mechanistic Insight into Surface-Initiated Polymerization of Methyl Methacrylate and Styrene via ATRP from Ordered Mesoporous Silica Particles

Pamela Pasetto,[†] Hélène Blas,[†] Fabrice Audouin,[†] Cédric Boissière,[‡] Clément Sanchez,[‡] Maud Save,*[,†,§] and Bernadette Charleux*[,†]

[†]*Laboratoire de Chimie des Polymères (UMR 7610) and* [‡]*Laboratoire de Chimie de la Matière Condensée (UMR 7574), UPMC and CNRS, Université Paris 6, 4 place Jussieu, 75252 PARIS Cedex 05, France.* [§]*Present address: IPREM Equipe Physique et Chimie des Polymères, UMR 5254, Université de Pau et des Pays de l'Adour and CNRS, Technopole Hélioparc, 2 Av Président Angot, 64053 PAU Cedex 9, France*

Received February 17, 2009; Revised Manuscript Received May 30, 2009

ABSTRACT: Hybrid materials were synthesized by grafting polymer chains from the surface of ordered mesoporous silica (OMS) particles via surface-initiated atom transfer radical polymerization (SI−ATRP) of methyl methacrylate or styrene. Various types of OMS particles were used as substrates: micrometric particles with ill-defined shape and varying mesopore diameters (9−14 nm), submicrometric polydisperse spherical OMS particles, and monodisperse core−shell particles composed of a dense silica core and an OMS shell, the latter two materials exhibiting ordered mesopores (diameter 2.5 nm) with radial orientation. This work proposes a systematic investigation of the molar mass, molar mass distribution and chain-end structure of both the grafted chains grown from the silica surface and the free chains produced in solution from an additional free initiator. The polymerizations of methyl methacrylate and styrene were perfectly controlled in the homogeneous medium via the ATRP mechanism whereas the study of the grafted chains highlighted the formation of a large fraction of dead species together with the expected population of living chains. The influence of the polymerization conditions and of the OMS particle structure on the occurrence of the extensive termination reactions was studied and discussed.

Introduction

Functionalization of mesostructured silica has attracted considerable research interest in the past few years due to their large specific surface area, high internal volume, narrow pore size distribution, and stable mesoporous structure.[1,2] Functional materials based on ordered mesoporous silica (OMS)[3] offer new potential applications, for instance, in the biomedical field, such as biocatalysis,[4] bone tissue engineering,[5] controlled drug delivery,[6] or stimuli-responsive nanovalves.[7] Polymer−silica composites structured by ordered mesoporous silica have also gained attention in the recent years for the development of specific materials for biomolecule adsorption,[8] enzyme immobilization,[9] temperature-responsive ibuprofen release,[10] thermosensitive vehicles for cellular imaging,[11] catalysis,[8] optoelectronic devices,[12] or the synthesis of mesoporous carbon via the carbonization of incorporated polyacrylonitrile.[13] Those materials were obtained either via in situ free-radical polymerization, after adsorption of vinyl monomers as a thin layer on the pore walls,[8,9,12] or via atom transfer radical polymerization initiated from the functional surface of the mesopores.[10,11,13]

Since the emergence of controlled/living free-radical polymerization (CRP)[14] techniques, the number of studies concerning the functionalization of inorganic surfaces via surface-initiated polymerization (the so-called *grafting from* method) has continuously increased. Indeed, the simultaneous growth of all polymer chains from the surface enables covalent attachment of a homogeneous polymer layer exhibiting high grafting density.[15−17] Among the CRP techniques, nitroxide-mediated radical polymerization (NMP),[18] atom transfer radical polymerization (ATRP)[19,20] and reversible addition−fragmentation chain transfer (RAFT)[21] are the most popular routes. The preparation of organic/inorganic nanocomposites via surface-initiated controlled free-radical polymerization (SI−CRP) through these techniques has been reviewed by several authors.[22−27] Among the various inorganic substrates used for grafting polymer chains via SI−CRP, colloidal silica particles have been extensively studied.[28−30] The best conditions to achieve a controlled/living free-radical polymerization were defined. In particular, in the case of ATRP and NMP, the addition of a sacrificial initiator solubilized in the continuous phase was shown to enhance the living character of the polymerization by favoring the production of deactivator (the so-called persistent radical effect[31]). Most of the studies demonstrated that the molar mass of the free chains produced by the sacrificial initiator matched those of the grafted chains, both types of chains exhibiting narrow molar mass distributions.[25] To a lesser extent, some research groups have been interested in the formation of polymer brushes via SI−CRP from ordered mesoporous silica. Most of the studies focused on SI−ATRP and various OMS particles synthesized with different templates were used as substrates, such as SBA-15 (SBA for Santa Barbara),[10,13,32] MCM-41 (MCM for Mobil composition of matter),[33] MSU (MSU for Michigan State University),[34] spherical OMS nanoparticles,[11] or even core−shell or hollow spherical OMS nanoparticles.[35] The preparation of nanocomposite materials from OMS (MCM-41) was also reported via SI−NMP[36] or via RAFT polymerization initiated from the outer surface of the particles.[37] However, in none of those studies related to SI−CRP from OMS substrates, the macromolecular features of the grafted chains were carefully studied. In a different way, Kruk et al.[38] very recently published

*Corresponding authors. E-mail: (M.S.) maud.save@univ-pau.fr; (B.C.) bernadette.charleux@upmc.fr. Telephone: +33 540175014.

Published on Web 07/22/2009

Table 1. Characteristics of the Ordered Mesoporous Silica (OMS) Particles

name	characteristics of silica particles	mesopore ordering	D^a (nm)	$S_{sp}{}^a$ ($m^2 \cdot g^{-1}$)	V^a ($cm^3 \cdot g^{-1}$)
MSU-Brij	ill-defined shape polydisperse (500 nm to 5 μm)	2D-hexagonal	14[b]	895	1.09
MSU-P123	ill-defined shape polydisperse (500 nm to 5 μm)	2D-hexagonal	9.9	455	0.61
SBA-15	ill-defined shape polydisperse (500 nm to 5 μm)	2D-hexagonal	9.0	490	0.97
MCM-41	spherical shape polydisperse (250−500 nm)	radial orientation	2.8	1150	0.68
CSSN-105	core−shell spherical nanoparticle monodisperse (< 600 nm)	radial orientation	2.5	560	0.40
CSSN-45	core−shell spherical nanoparticle monodisperse (< 500 nm)	radial orientation	2.2	265	0.23
CSSN-30	core−shell spherical nanoparticle monodisperse (< 500 nm)	radial orientation	2.7	207	0.16

[a] Data measured by nitrogen adsorption: D = mesopore diameter; S_{sp} = specific surface area; V = pore volume. [b] Presence of a double porosity: 7 v-% of mesopores with 5 nm diameter and 93 v-% of mesopores with 14 nm diameter.

on ATRP of acrylonitrile, styrene, and dimethylaminoethyl methacrylate (DMAEMA) initiated from the surface of ordered mesoporous silica particles with mesopore diameters in the 10−15 nm range, for the purpose of giving more complete information on the controlled polymerization characteristics. In particular, they showed that the SI−ATRP of acrylonitrile was perfectly controlled but that the polydispersity of the grafted polystyrene chains increased significantly with conversion (up to 2.1−2.9) and that the analysis of the PDMAEMA cleaved chains was unsuccessful, presumably due to the protonation of the amino groups during hydrolysis of the silica.[38]

The lack of more conclusive information on the living character of the chains produced via SI−ATRP from OMS surfaces prompted us to investigate the ATRP of methyl methacrylate (MMA) and styrene (S) initiated from the surface of OMS particles with different morphologies and different pore sizes. Our aim was to study the impact of the confined mesopore space on the polymer characteristics. In this context, Genzer et al.[39] suggested an influence of the concave substrate geometry on the polydispersity of chains grafted via SI−ATRP. Kitagawa et al.[40] showed the impact of microchannel size (diameter < 1 nm) on the polydispersity, tacticity and branching of polymers synthesized by conventional radical polymerization performed inside the microporous structure. For the present investigation, we used various types of ordered mesoporous silica particles, all of them exhibiting mesopores with cylindrical shape: (i) micrometric particles with an ill-defined shape but a perfect hexagonal ordering of the mesopores with average diameters ranging between 9 and 14 nm and large, polydisperse lengths; (ii) submicrometric, polydisperse, spherical OMS particles with 2.5 nm diameter mesopores exhibiting a radial orientation; (iii) submicrometric monodisperse spherical core−shell particles composed of a spherical silica core and an OMS shell with ordered mesopores (diameter 2.5 nm) of short monodisperse length (varying from 30 to 105 nm), oriented perpendicular to the core surface. The objective was to perform SI−ATRP from the different substrates and to thoroughly analyze the macromolecular features of both the free and grafted chains by size exclusion chromatography and mass spectrometry analyses.

Experimental Section

Materials. Methyl methacrylate (Aldrich, 99%), styrene (Acros, 99%), toluene and triethylamine were distilled from calcium hydride prior to use. All other reagents, tetraethoxysilane (TEOS, Fluka, > 99%), cetyltrimethylammonium bromide (CTAB, Aldrich, 99%), Pluronic P123 (poly(ethylene oxide)-*b*-poly(propylene oxide)-*b*-poly(ethylene oxide) triblock copolymer, $M_n \approx 5800\ g \cdot mol^{-1}$, Aldrich), Brij 56 (polyethylene glycol hexadecyl ether, $M_n \approx 680\ g \cdot mol^{-1}$, Aldrich), ammonium fluoride (NH_4F, Merck), sodium fluoride (NaF, Prolabo, 98%), 5-hexen-1-ol (Alfa Aesar, 97%), 2-bromoisobutyryl bromide (Alfa Aesar, 97%), chlorodimethylsilane (Alfa Aesar, 97%), dihydrogenhexachloroplatinate hexahydrate (H_2PtCl_6, 6 H_2O, ABCR, 99%), ethyl-2-bromoisobutyrate (EBiB, Alfa Aesar, 98%), ethyl-2-bromopropionate (EBP, Alfa Aesar, 98%), Cu(I)Cl (Aldrich, 99%), Cu(II)Cl_2 (Acros, 98%), Cu(I)Br (Aldrich, 99%), Cu(II)Br_2 (Acros, 98%), 1,1,4,7,10,10-hexamethyltriethylenetetramine (HMTETA, Aldrich, 97%), *N*,*N*′,*N*′,*N*″-pentamethyldiethylenetriamine (PMDETA, Aldrich, 99%), and dimethylformamide (DMF) (Carlo Erba, 99.9%) were used as received.

Preparation of Ordered Mesoporous Silica (OMS) Particles. The various OMS particles (i.e., MSU-P123, MSU-Brij, SBA-15, and MCM-41) were synthesized according to published protocols[41−43] and the experimental procedures are detailed in the Supporting Information.

The core−shell spherical silica nanoparticles (CSSN) with dense silica core and ordered mesoporous silica shell with mesopores oriented perpendicular to the surface were synthesized via a two-step procedure.[44] First, the spherical dense core was prepared via the Stöber protocol (see SN-1 and SN-2 in the Supporting Information file). Then, formation of the mesoporous shell was performed as follows. For the CSSN-45 particles, a mixture of 400 mL of water and 60 mL of CTAB solution (110 mM, 40 mL water, 20 mL ethanol) was prepared. The crude suspension (200 mL) of the core spherical silica nanoparticles (SN-1) was added to the prepared mixture and stirred for 30 min at room temperature. Then, TEOS (4.0 g) was slowly introduced and the reaction was performed at room temperature overnight. The TEOS:CTAB:NH_3:EtOH:H_2O molar ratio used in the present synthesis was 1:0.34:7.0:210:1325. The average thickness of the OMS shell was 45 nm. The CSSN-30 and CSSN-105 materials were synthesized according to a similar procedure using different volumes of the "TEOS:CTAB:NH_3:EtOH:H_2O" solution and a constant volume of the SN-2 suspension of Stöber particles. The average thicknesses of the OMS shell were 30 and 105 nm for the CSSN-30 and CSSN-105 particles, respectively.

For all silica nanoparticle syntheses (see summary in Table 1), the precipitated powders were separated from the solution by filtration on a Durapore GS filter or by centrifugation, dried one night at 80 °C and calcined at 500 °C for one night (heating ramp 5 °C/min).

Grafting of the ATRP Initiator onto the Silica Surface. The silylated initiator (see the Supporting Information for the synthesis protocol) was mixed with dry toluene and the solution was transferred through nitrogen flow into a purged flask containing the mesoporous silica and dry triethylamine. In a general procedure, the number of moles of initiator introduced was half the theoretical number of surface hydroxyl group (considered at 5 OH/nm^2) and three molar excess of triethylamine

Table 2. Characteristics of the initiator-functionalized silica particles

initiator-functionalized silica[a]	$W\%_{silica}$[b] crude silica	$W\%_{initiator+silica}$[b] initiator-based silica	G_I[c] (initiator·nm^{-2})
MSU-P123-BiB	6.7	16.6	0.6
SBA-15-BiB	3.3	25.1	1.3
MCM-41-BiB	5.5	21.6	0.4
CSSN-105-BiB	3.0	23.3	1.0
CSSN-45-BiB	4.5	16.3	1.2
CSSN-30-BiB	1.6	11.7	1.3
SN-1-BiB (Stöber particles)	0.6	1.6	2.1[d]
MSU-Brij-BP	1.5	27.8	0.9
MSU-P123-BP	6.1	17.0	0.7

[a] BiB = bromoisobutyrate; BP = bromopropionate [b] $W\%$ = weight loss between 120 and 800 °C (TGA analysis). [c] Initiator grafting density (molecule·nm^{-2}) (see Experimental Section, eq 1). [d] The weight loss observed in TGA being low for the Stöber particles, the presence of the grafted initiator was confirmed by elemental analysis (C 0.99%, Br 0.20%, Si 43.41%) and the initiator grafting density was calculated according to the equation previously published by Bartholome et al.:[29] $G_I = 1.5$ initiator·nm^{-2}.

Table 3. Experimental Conditions Used for SI−ATRP of MMA from Stöber and OMS Particles Grafted with Bromoisobutyrate Initiator (BiB)[a]

expt	functionalized silica	τ_{silica}[b]	$[BiB]_g$[c] (mol·L^{-1})	$[EBIB]_f$[c] (mol·L^{-1})	$[MMA]/([BiB]_g + [EBiB]_f)$[d]
1	none			2.29×10^{-2}	200
2	MSU-P123-BiB	1.7	8.3×10^{-3}	1.46×10^{-2}	200
3	SBA-15-BiB	0.8	7.99×10^{-3}	1.33×10^{-2}	200
4	MSU-P123-BiB	1.4	9.20×10^{-3}	1.40×10^{-2}	200
5	SN-1-BiB	4.7	1.59×10^{-3}	1.61×10^{-2}	241
6	CSSN-30-BiB	2.2	8.56×10^{-3}	3.72×10^{-3}	348
7	CSSN-45-BiB	1.8	1.17×10^{-2}	1.58×10^{-2}	162
8	CSSN-105-BiB	0.8	7.85×10^{-3}	3.73×10^{-3}	369
9	MCM-41-BiB	1.8	1.18×10^{-2}	1.09×10^{-2}	200
10	MSU-P123-BiB	1.8	8.4×10^{-3}	0	549
11	CSSN-30-BiB	2.4	9.44×10^{-3}	0	449
12	CSSN-45-BiB	3.9	2.69×10^{-2}	0	157
13	CSSN-105-BiB	1.3	1.22×10^{-2}	0	350
14	MCM-41-BiB	1.7	1.19×10^{-2}	0	385

[a] $[MMA] = 4.4 \pm 0.2$ mol·L^{-1}; $[DMF] = 0.65 \pm 0.15$ mol·L^{-1}; [BiB+EBiB]:[HMTETA]:[CuCl]:[$CuCl_2$] = 1:1:0.80:0.20; $T = 90$ °C; MMA:toluene = 50:50 (wt:wt). [b] $\tau_{silica} = 100 \times m_{silica}/m_{total}$ is the weight content of silica in the polymerization medium with m_{silica} being the mass of OMS particles and m_{total} being the mass of all the introduced compounds. [c] $[BiB]_g$ and $[EBiB]_f$ correspond to the concentrations of the grafted BiB initiator and the free EBiB initiator respectively, calculated for the whole reaction medium volume. [d] $[MMA]/([BiB]_g + [EBiB]_f)$ ratio corresponds to the theoretical number-average degree of polymerization (DP_n).

Table 4. Experimental Conditions Used for SI−ATRP of Styrene from OMS Particles Grafted with Bromopropionate Initiator (BP) in the Presence of Ethyl-2-bromopropionate (EBP) as Free Initiator[a]

expt	functionalized silica	τ_{silica}[b]	$[BP]_g$[c] (mol·L^{-1})	$[EBP]_f$[c] (mol·L^{-1})	$[S]/([BiB]_g + [EBiB]_f)$[d]
15	MSU-P123-BP	1.5	8.9×10^{-3}	2.9×10^{-2}	200
16	MSU-Brij-BP	0.9	1.1×10^{-2}	2.0×10^{-2}	200
17	MSU-Brij-BP	1.7	2.2×10^{-2}	4.9×10^{-2}	110

[a] [styrene] = 7.7 mol·L^{-1}; [DMF] = 1.1 mol·L^{-1}; [BP+EBP]: [PMDETA]:[CuBr]: [$CuBr_2$] = 1: 1: 0.9:0.1; $T = 90$ °C. [b] $\tau_{silica} = 100 \times m_{silica}/m_{total}$ is the weight content of silica in the polymerization medium with m_{silica} the mass of OMS particles and m_{total} the mass of all the introduced compounds. [c] $[BP]_g$ and $[EBP]_f$ correspond to the concentrations of the grafted BP initiator and the free EBP initiator respectively, calculated for the whole reaction medium volume. [d] The $[S]/([BiB]_g + [EBiB]_f)$ ratio corresponds to the theoretical number-average degree of polymerization (DP_n).

was used. The mixture was stirred for 16 h at 50 °C and the ungrafted molecules were removed from the powder by centrifugation in methanol first and dichloromethane afterward. The initiator grafting density (G_I) is calculated according to eq 1.

$$G_I = \frac{\frac{W\%_{initiator+silica}}{100 - W\%_{initiator+silica}} - \frac{W\%_{silica}}{100 - W\%_{silica}}}{M_{initiator} \times S_{sp}} \times N_A \text{ (molecule/nm}^2\text{)} \quad (1)$$

$W\%$ is the weight loss between 120 and 800 °C (TGA analysis), N_A is the Avogadro's number, $M_{initiator}$ is the molar mass of the initiator calculated by subtracting the molar mass of the Si and Cl atoms ($M_{initiator} = 280$ and 266 g·mol^{-1} for the isobutyrate-based initiator and the propionate-based initiator, respectively), and S_{sp} is the specific surface area. The values of G_I for all the initiator-functionalized silica particles are reported in Table 2.

Procedure for Surface-Initiated ATRP of Methyl Methacrylate and Styrene. The detailed experimental conditions for all polymerizations are gathered in Table 3 for MMA and in Table 4 for S. In a typical experiment (expt 14, Table 3), the initiator-grafted mesoporous silica particles (0.41 g, 2.9×10^{-4} mol initiator) and copper catalyst (23 mg CuCl, 2.3×10^{-4} mol and 7.8 mg $CuCl_2$, 5.8×10^{-5} mol) were poured into a round-bottom flask equipped with a rubber septum and subsequently purged by two vacuum-nitrogen cycles. In a separate flask sealed with a rubber septum, the mixture containing methyl methacrylate (11 g, 1.1×10^{-1} mol), DMF (1.4 g, 10 wt.-% vs MMA), HMTETA (67 mg, 2.9×10^{-4} mol), toluene (9.3 g) and for some experiments the required amount of "free" sacrificial initiator was degassed by nitrogen bubbling for 30 min before being introduced under nitrogen atmosphere via a canula into the flask containing the silica particles. For an experiment carried out in the presence of free initiator (expt 9, Table 3), 52 mg of EBiB (2.7×10^{-4} mol) was added to the mixture of liquids containing 11 g of MMA, 1.4 g of DMF, 9.3 g of toluene, and 130 mg of HMTETA. The solids content of silica versus liquids ranged between 1 and 4.7 wt %. The polymerization was carried out at 90 °C for the required time of polymerization and aliquots of serum were withdrawn at regular time intervals for kinetic analysis. Monomer conversion was calculated from the proton NMR spectrum of a raw aliquot using DMF as an internal standard (see Supporting Information for the exact resonances, Figure SI-2 and Figure SI-3). The copper catalyst was removed from the free polymer by passing the supernatant

solution diluted with dichloromethane through an alumina column. The solvents were evaporated and the free polymer chains were dissolved in THF for SEC analysis. The hybrid materials were carefully washed before any further treatment or characterization. The nongrafted species (polymer, catalyst, initiator, monomer) were removed by either Soxhlet extraction with dichloromethane and methanol in the case of micrometric particles or by 10 centrifugation-solvent exchange cycles in the case of submicrometric spherical particles. The grafted polymer chains were cleaved from the silica surface using fluorhydric acid according to the procedure described in ref 45. Dichloromethane was then added and fluorhydric acid was extracted with water until neutral pH. The organic solution containing the cleaved polymer chains was dried over magnesium sulfate, filtered, evaporated and the recovered polymer was mixed with the appropriate amount of THF for subsequent SEC analysis. To analyze both the free chains and the grafted ones as a function of conversion, the ATRP of MMA initiated from MSU P123-BiB particles in the presence of free initiator (expt 2 in Table 3) was carried out in 3 different flasks and the polymerization was stopped at different time intervals.

The polymer grafting density (G_P) was calculated according to eq 2.

$$G_P = \frac{\frac{W\%_{polymer+initiator+silica}}{100-W\%_{polymer+initiator+silica}} - \frac{W\%_{silica+initiator}}{100-W\%_{silica+initiator}}}{M_{n,\,grafted-polymer} \times S_{sp}} \times N_A \quad (chain/nm^2) \qquad (2)$$

W % is the weight loss between 120 and 800 °C (TGA analysis) and $M_{n,grafted\text{-}polymer}$ is the number average molar mass of the grafted chains.

Characterization Methods. Proton (250 MHz) and carbon (62.5 MHz) NMR analyses were performed in $CDCl_3$ using an AC250 Brucker spectrometer.

The number-average molar mass (M_n), the weight-average molar mass (M_w) and the molar mass distributions (polydispersity index PDI = M_w/M_n) of the obtained poly(methyl methacrylate) and polystyrene were determined by size exclusion chromatography (SEC) using tetrahydrofuran (THF) as an eluent at a flow rate of 1 mL·min^{-1}. The SEC apparatus was equipped with a Viscotek VE 5200 automatic injector, two columns thermostatted at 40 °C (PSS SDV, linear M, 8 mm × 300 mm, particle size: 5 μm, mixed bed columns, separation range 100 − 1 000 000 g·mol^{-1}) and a differential refractive index detector (LDC Analytical refractoMonitor IV). The average molar masses were derived from a calibration curve based on poly(methyl methacrylate) standards from Polymer Standards Service (separation limits: 200 to 1.94 × 10^6 g·mol^{-1}) for PMMA and from a calibration curve based on polystyrene standards from Polymer Standards Service (separation limits: 260 to 2 × 10^6 g·mol^{-1}) for PS.

Fractionation of the polymers was performed by semipreparative SEC using a Waters apparatus equipped with three columns (UltraStyragel 19 × 300 mm, 500, 10^3, 10^4 Å). The eluent was tetrahydrofuran at a flow rate of 5 mL·min^{-1}. A 200 μL portion of a polymer solution at 30 g·L^{-1} was injected. A differential refractive index detector was used, and molar masses were derived from a calibration curve based on poly(methyl methacrylate) standards (see characteristics above).

Matrix-assisted laser desorption ionization−time-of-flight mass spectrometry (MALDI−TOF MS) was performed using a PerSeptive Biosystems Voyager Elite (Framingham, MA) time-of-flight mass spectrometer equipped with a nitrogen laser (337 nm). It was operated at an accelerating potential of 20 kV either in reflector or in linear mode using a low power for the laser (1800 or 2000). The MALDI−TOF mass spectra represent averages over 256 shots (3 Hz repetition). To prepare the polymer solution, THF was added to the sample to reach a concentration between 0.5 and 2 g·L^{-1}. The matrix, 1,8-dihydroxy-9[10*H*]-anthracenone (dithranol), was also dissolved in THF (25 g·L^{-1}). A 10 μL portion of the polymer solution was mixed with 20 μL of the matrix solution. A sodium iodide solution (10 μL of a solution at 20 g·L^{-1} in THF) was finally added to favor ionization by cation attachment. A 1 μL portion of the final solution was deposited onto the sample target and allowed to dry in air at room temperature. Polystyrene standards were used for the calibration.

Thermogravimetric analyses (TGA) were performed on a TGA Q50 from TA Instrument using a temperature ramp from 20 to 800 °C at 20 °C/min (the weight loss is denoted W %). Fourier transform infrared (FTIR) spectra were recorded from KBr pellets at room temperature using a Nicolet Avatar FTIR spectrometer. Transmission electron microscopy (TEM) images were taken with a JEOL JEM 100CX II (100 kV) instrument. The samples dispersed in ethanol were dropped onto a carbon copper grid and dried before TEM analysis. Powder X-ray diffraction (XRD) patterns were recorded by using a conventional diffractometer (Philips PW1820) operating in reflection geometry ($\theta-2\theta$ mode) with Cu Kα radiation (λ = 0.15418 nm). Materials porosity was characterized by N_2 adsorption/desorption curves obtained with a Micromeritics ASAP2010 apparatus. Surface area value and pore size distribution were obtained with the corrected BET equation and Broekhoff and de Boer models respectively.[46] All measurements were performed on calcined powders.

Results and Discussion

1. Synthesis and Functionalization of Ordered Mesoporous Silica Particles. The elaboration of ordered mesoporous silica particles exhibiting cylindrical mesopores with various diameters was performed via hydrolysis/condensation of tetraethoxysilane in the presence of either cetyltrimethylammonium bromide (CTAB), poly(ethylene oxide) hexadecyl ether (Brij 56), or poly(ethylene oxide)-*b*-poly(propylene oxide)-*b*-poly(ethylene oxide) triblock copolymer (Pluronic P123) used as templates (Table 1). The shape of the micrometric particles was ill-defined (see Figure 1) but an ordered arrangement of the cylindrical mesopores with a narrow pore size distribution was observed by transmission electron microscopy (Figure 1). In addition, their powder X-ray diffractogram (XRD) clearly indicated a two-dimensional hexagonal ordering of the mesopores (Figure SI-1a). After grafting of the ATRP initiator, the analysis showed that the ordered structure was maintained (Figure SI-1a). The micrometric silica particles (MSU-P123, MSU-Brij and SBA-15) exhibited pore diameters ranging from 9.0 to 14 nm and BET specific surface areas ranging from 455 to 895 m^2 g^{-1} (Table 1).

The synthesis of well-defined submicrometric spherical OMS particles (diameter below 600 nm) was performed to design a series of particles exhibiting an increasing ratio of the overall specific surface area over the external surface area. For that purpose, we synthesized either entirely mesoporous spherical particles (MCM-41, Figure 1) or monodisperse core−shell spherical particles composed of dense silica core and OMS shell with ordered mesopores oriented perpendicular to the core surface (CSSN, Figure 1). Core−shell particles with varying OMS shell thicknesses were successfully synthesized at basic pH in the presence of CTAB as a template (see Figure 1: CSSN-30, CSSN-45, CSSN-105). The nitrogen adsorption isotherms of the spherical OMS particles are displayed in Figure 2 and the values of the specific surface areas and the pore volumes are gathered in Table 1. The presence of the XRD peak confirmed the

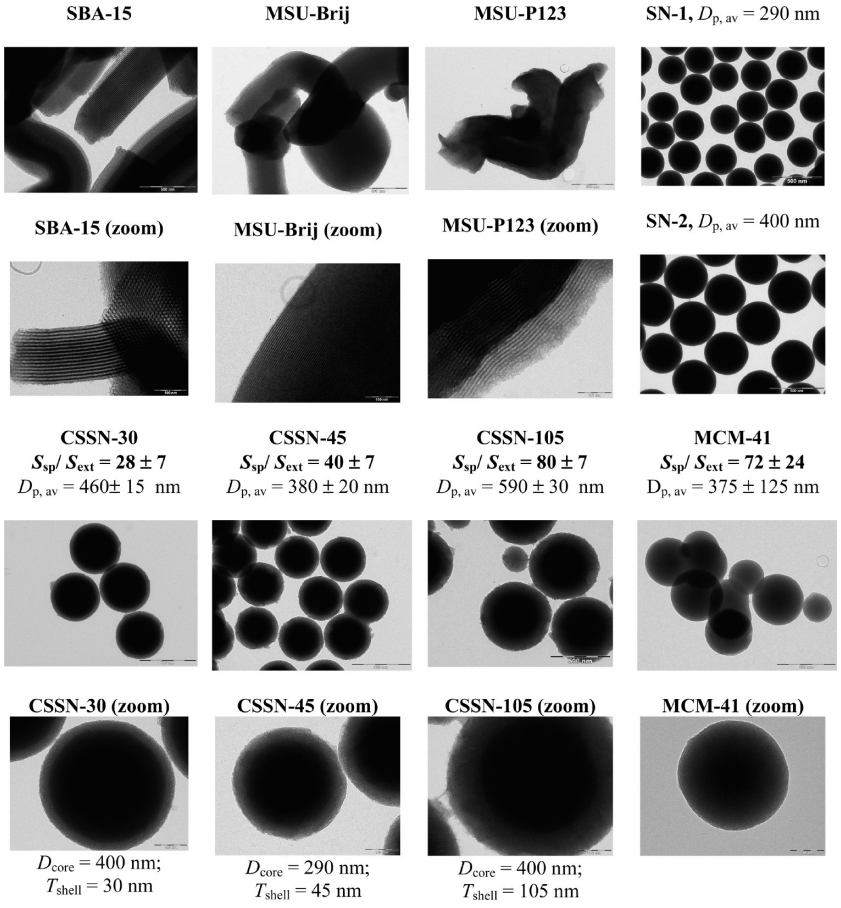

Figure 1. Transmission Electron Micrographs (TEM) of OMS particles with various morphologies: micrometric OMS particles (SBA-15, MSU-Brij, MSU-P123); Stöber spherical nanoparticles (SN-1 and SN-2); core−shell spherical nanoparticles with OMS shell and dense silica core (CSSN-30, CSSN-45, CSSN-105); spherical OMS particles (MCM-41). S_{sp}/S_{ext} corresponds to the ratio of the specific surface area over the external surface area; $D_{p,av}$ = average particle diameter; D_{core} = core diameter; T_{shell} = thickness of the OMS shell. The scale bars correspond to 500 nm for the TEM pictures of OMS particles and to 100 nm for zooms.

mesopore ordering (Figure SI-1b) but the arrangement of the mesopores exhibiting a radial orientation, the two-dimensional hexagonal ordering was not observed. The average mesopore diameter was around 2.5 nm for all submicrometric spherical particles (Table 1).

After calcination, the ordered mesoporous silica particles were functionalized by grafting either (6-dimethylchlorosilylhexyl)-2-bromoisobutyrate or (6-dimethylchlorosilylhexyl)-2-bromopropionate initiator for the subsequent ATRP of methyl methacrylate and styrene respectively (see the experimental part and Scheme 1). Monochlorosilane-based molecules were selected in order to promote the formation of a monolayer by condensation with the surface hydroxyl groups, hence avoiding co-condensation reactions between initiator molecules. The success of the grafting was first confirmed by the presence of the characteristic absorption band of the aliphatic ester group (1750 cm^{-1}) on the FTIR spectrum (Figure SI-4a). The weight loss measured by thermogravimetric analysis enabled us to calculate the initiator grafting density (G_I) and the corresponding values ranged between 0.4 and 1.3 molecules.nm^{-2} (see Table 2). These values are similar to those previously published for the grafting of such molecules onto colloidal silica particles.[47,48] The initiator grafting density was calculated on the basis of the overall specific surface area of the material, which confirms the efficient grafting of the initiator inside the mesopores. We deliberately chose to modify the silica surface with the ATRP initiator only and not with an additional inert

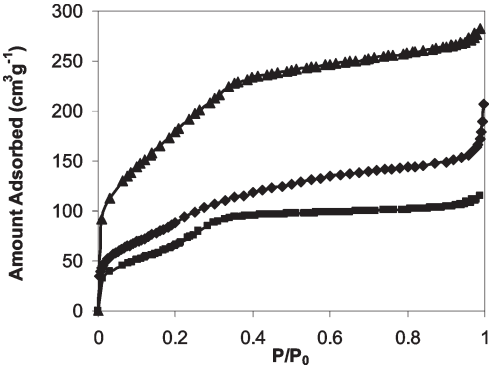

Figure 2. Overlay of nitrogen adsorption isotherms according to the relative pressure P/P_0 for CSSN-105 (▲), CSSN-45 (♦), and CSSN-30 (■).

hydrophobic molecule, as done previously by Kruk et al.[38] Our aim was to provide a direct comparison with the majority of the published SI−ATRP results from silica surfaces.

2. Surface-Initiated ATRP of Methyl Methacrylate and Styrene from OMS Particles. The OMS particles served as substrate for the ATRP of methyl methacrylate and styrene using copper catalysts as activator and deactivator, i.e., $CuCl/CuCl_2$/HMTETA for MMA and $CuBr/CuBr_2$/PMDETA for styrene. The experiments were performed

Scheme 1. Synthetic Route for SI−ATRP of MMA and Styrene from OMS Particles: (A) Esterification, (B) Hydrosilylation, (C) Grafting of the Initiator, and (D) Polymerization

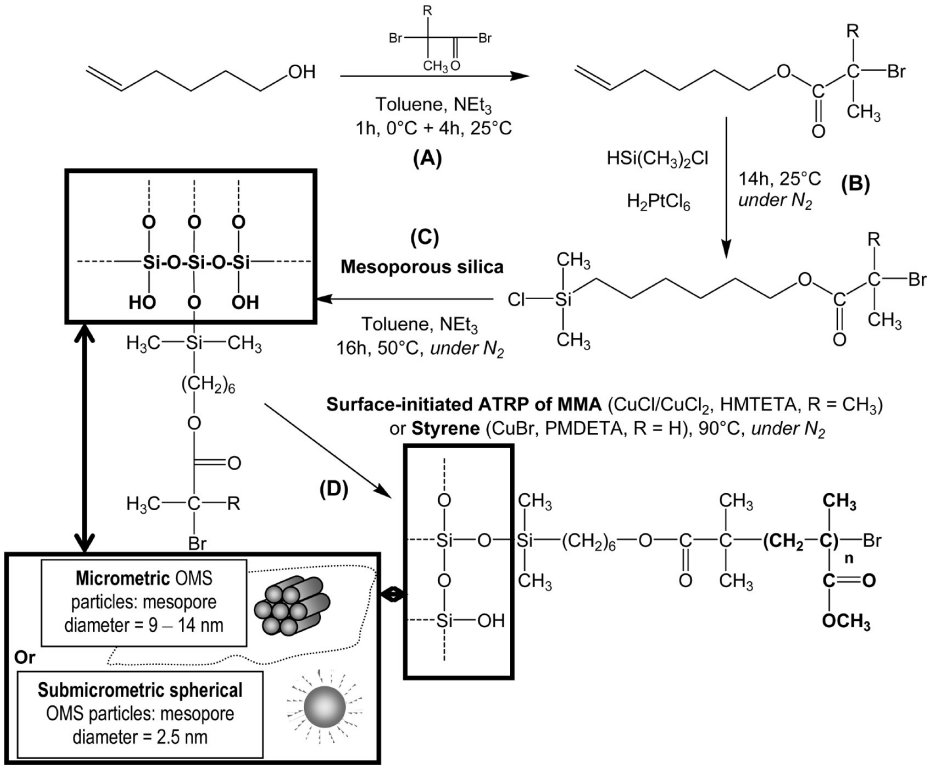

Table 5. Surface-Initiated Polymerization of MMA from Silica Particles Grafted with Bromoisobutyrate Initiator (BiB) in the Presence of Ethyl-2-bromoisobutyrate (EBiB) as Free Initiator[a]

						free chains		grafted chains		
expt	functionalized silica	$W\%_{PMMA}$[b]	mol % free initiator[c]	% convn (time/h)	$M_{n,theo}$[d] ($g\cdot mol^{-1}$)	$M_{n,SEC}$ ($g\cdot mol^{-1}$)	M_w/M_n	$M_{n,SEC}$ ($g\cdot mol^{-1}$)	M_w/M_n	G_P[e] (chain. nm^{-2})
1	none		100	82 (6)	16 600	26 600	1.07			
2	MSU-P123-BiB	24	63	73 (6)	14 700	30 600	1.07	3400 multimodal	4.6	[g]
5	SN-1-BiB	7	90	71 (7)	17 330	20 550	1.14	17 890	1.2	0.29
6	CSSN-30-BiB	35	30	77 (7.1)	23 530	63 730	1.12	43 720	1.4	0.05
7	CSSN-45-BiB	23	57	97 (6.6)	15 930	19 870	1.15	16 920	1.4	0.06
8	CSSN-105-BiB	26	30	33 (6.7)	12 400	35 270	1.31	11 675	2.9	[g]
9	MCM-41-BiB	27	48	94 (22)	19 020	40 870	1.16	4000 multimodal	6.9	[g]

[a] [MMA] = 4.4 ± 0.2 mol·L^{-1}; [DMF] = 0.65 ± 0.15 mol·L^{-1}; [BIB+EBiB]:[HMTETA]:[CuCl]:[$CuCl_2$] = 1:1:0.80:0.20; T = 90 °C; MMA: toluene = 50:50 (wt:wt). See further experimental details in Table 3. [b] Weight amount of PMMA ($W\%_{PMMA} = W\%_{PMMA+initiator+silica} - W\%_{initiator+silica}$, with W % being the weight loss between 120 and 800 °C from TGA). [c] Molar fraction of free initiator (%) = 100 × [free initiator]$_0$/([free initiator]$_0$ + [grafted initiator]$_0$). [d] Theoretical molar mass: $M_n = M_{initiator} + M_{MMA} \times$ conversion × [MMA]$_0$/[grafted initiator + free initiator]$_0$ [e] Polymer grafting density (chain·nm^{-2}) using $M_{n,grafted\text{-}polymer}$, the average molar mass of the grafted chain (see Experimental Section, eq 2). [g] The molar mass distribution of the grafted chains being broad with the presence of low molar mass tail, this calculation was not performed due to the lack of accuracy.

Table 6. Surface-Initiated Polymerization of MMA from OMS Particles Grafted with Bromoisobutyrate Initiator (BiB) in the Absence of Free Initiator[a]

					grafted chains			
expt	silica	$W\%_{PMMA}$[b]	% convn (time /h)	$M_{n,theo}$[c] ($g\cdot mol^{-1}$)	$M_{n,SEC}$ ($g\cdot mol^{-1}$)	M_w/M_n	G_P[d] (chain·nm^{-2})	$M_{n,theo}/M_{n,SEC}$
10	MSU-P123-BiB	35	10 (7.0)	5300	4500	13.4	[e]	[e]
11	CSSN-30-BiB	27	12 (7.1)	5600	24 040	2.0	0.06	0.23
12	*CSSN-45-BiB*	46	30 (7.4)	7180	54 220	1.6	0.05	0.13
13	CSSN-105-BiB	39	14 (8.0)	5370	30 180	2.4	0.05	0.17
14	MCM-41-BiB	39	23 (7.2)	9000	8600	9.7	[e]	[e]

[a] [MMA] = 4.4 ± 0.2 mol·L^{-1}; [DMF] = 0.65 ± 0.15 mol·L^{-1}; [BiB]$_g$:[HMTETA]:[CuCl]:[$CuCl_2$] = 1:1:0.80:0.20; T = 90 °C; MMA: toluene = 50:50 (wt:wt). See further experimental details in Table 3. [b] Weight amount of PMMA ($W\%_{PMMA} = W\%_{PMMA+initiator+silica} - W\%_{initiator+silica}$, with W % the weight loss between 120 and 800 °C from TGA). [c] Theoretical molar mass: $M_n = M_{initiator} + M_{MMA} \times$ conversion × [MMA]$_0$/[Grafted initiator]$_0$ [d] Polymer grafting density (chain/nm^2) with $M_{n,grafted\text{-}polymer}$ the average molar mass of the grafted chain (see Experimental Section, eq 2). [e] The molor mass distribution of the grafted chains being broad with the presence of a low molor mass tail, this calculation was not performed due to the lack of accuracy.

Table 7. Surface-Initiated Polymerization of Styrene from Silica Particles Grafted with Bromopropionate Initiator (BP) in the Presence of Ethyl-2-bromopropionate (EBP) as Free Initiator[a]

						free chains		grafted chains	
expt	functionalized silica	$W\%_{PS}$[b]	mol % free initiator[c]	% convn (time/h)	$M_{n,theo}$[d] ($g \cdot mol^{-1}$)	$M_{n,SEC}$ ($g \cdot mol^{-1}$)	M_w/M_n	$M_{n,SEC}$ ($g \cdot mol^{-1}$)	M_w/M_n
15	MSU-P123-BP	34	76	58 (6.5)	12 500	18 920	1.15	3270	9.7
16	MSU-Brij-BP	25	67	67 (6)	14 110	28 670	1.11	2630	4.7
17	MSU-Brij-BP	25	69	67 (7)	7840	11 040	1.12	1550	3.2

[a] [S] = 7.7 mol·L^{-1}; [DMF] = 1.1 mol·L^{-1}; [BP+EBP]:[PMDETA]:[CuBr]: [$CuBr_2$] = 1: 1: 0.9: 0.1; T = 90 °C. See further experimental details in Table 4. [b] Weight amount of PS ($W\%_{PS} = W\%_{PS+initiator+silica} - W\%_{initiator+silica}$, with $W\%$ the weight loss between 120 and 800 °C from TGA). [c] [free initiator]$_0$ × 100/([free initiator]$_0$ + [grafted initiator]$_0$). [d] Theoretical molar mass: $M_n = M_{initiator} + M_S \times$ conversion × [S]$_0$/[grafted initiator + free initiator]$_0$

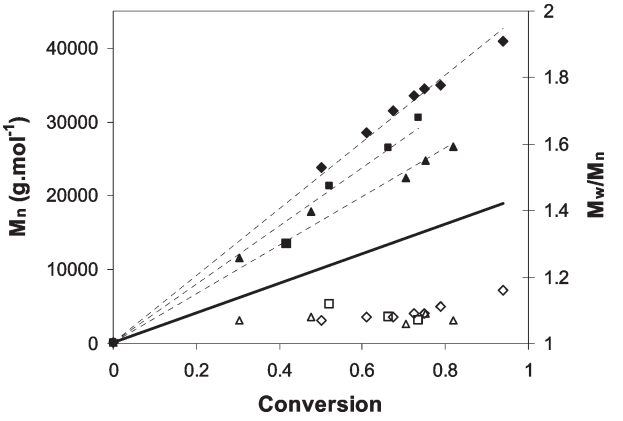

Figure 3. Number-average molar mass (M_n, plain symbols) and polydispersity index (PDI = M_w/M_n, empty symbols) of the free polymer chains as a function of monomer conversion. ATRP of MMA carried out in the absence of silica particles (▲, △, expt 1, fraction of grafted initiator = 0 mol %, initiator efficiency f = 0.61) and in the presence of both free initiator and either MSU-P123-BiB functionalized OMS particles (■, □, expt 2, fraction of grafted initiator = 36 mol %, f = 0.51) or MCM-41-BiB functionalized OMS particles (◆, ◇, expt 9, fraction of grafted initiator = 52 mol %, f = 0.44). See experiments in Tables 3 and 5. The full straight line corresponds to the theoretical M_n vs conversion.

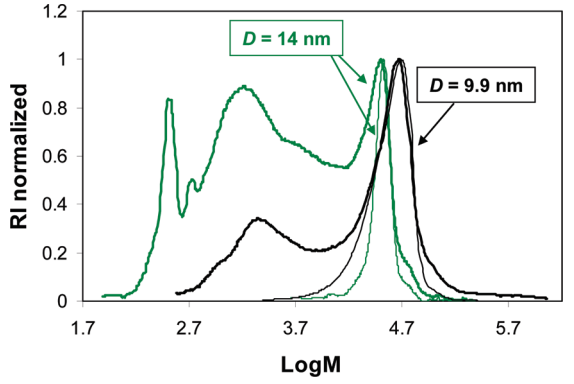

Figure 4. Surface-initiated ATRP of styrene from MSU-P123-BP OMS particles (mesopore diameter = 9.9 nm, expt 15, black lines) and from MSU-Brij-BP OMS particles (mesopore diameter = 14 nm, expt 16, green lines): influence of the average mesopore diameter on the SEC chromatograms of cleaved chains (thick line) and free chains (thin line). See Tables 4 and 7.

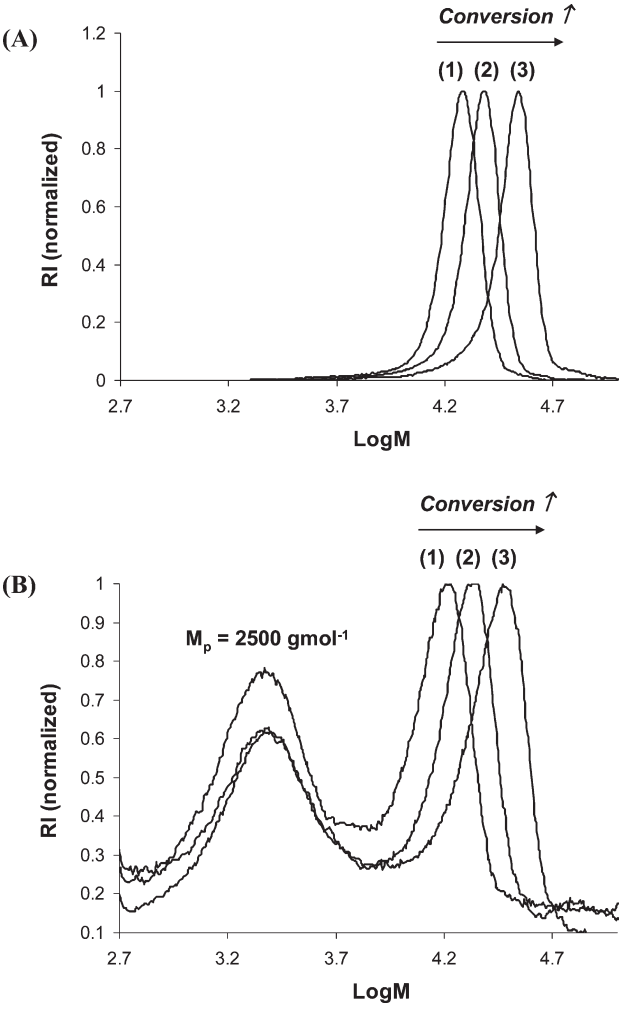

Figure 5. Surface-initiated ATRP of MMA from the micrometric MSU-P123-BiB OMS particles (mesopore diameter 9.9 nm) (expt 2 in Table 3). (A) SEC chromatograms of the free chains for three different monomer conversions (%): (1) 50%, M_n = 21 150 g·mol^{-1}, M_w/M_n = 1.06; (2) 62%, M_n = 22 230 g·mol^{-1}, M_w/M_n = 1.06. (**3**) 91%, M_n = 34 040 g·mol^{-1}, M_w/M_n = 1.06. (B) SEC chromatograms of the cleaved chains for three different monomer conversions (%), evolution of M_p (molar mass at the peak maximum) of the "living" chains: (1) 50%, $M_p \approx$ 16 320 g·mol^{-1}; (2) 62%, $M_p \approx$ 21 880 g·mol^{-1}; (3) 91%, $M_p \approx$ 30 020 g·mol^{-1}.

either in the presence or in the absence of free initiator as described in the Experimental Section. The first method is very useful for a mechanistic investigation as the analysis of the free chains allows a comparison with the macromolecular features of the grafted chains. It also provides indication on the quality of the polymerization control in the homogeneous medium in the presence of the OMS particles. The controlled growth of polymer chains via ATRP requires a minimum amount of deactivator in order to reversibly deactivate the growing polymer chains, especially for SI−ATRP performed in the absence of free initiator as the amount of deactivator produced by the persistent radical effect[31] might not be sufficient.[49] Cu(II) halide deactivator

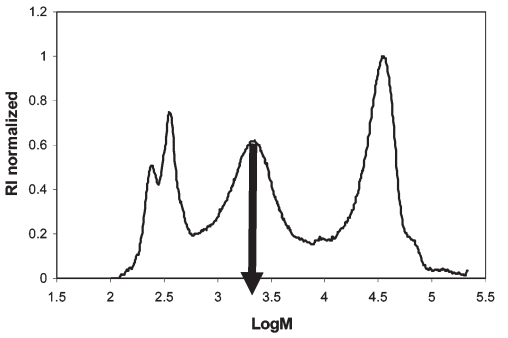

Characteristics of the analyzed PMMA fraction	M_n (g·mol^{-1})	M_w/M_n
SEC	2 450	1.02
MALDI-TOF MS	2 300	1.01

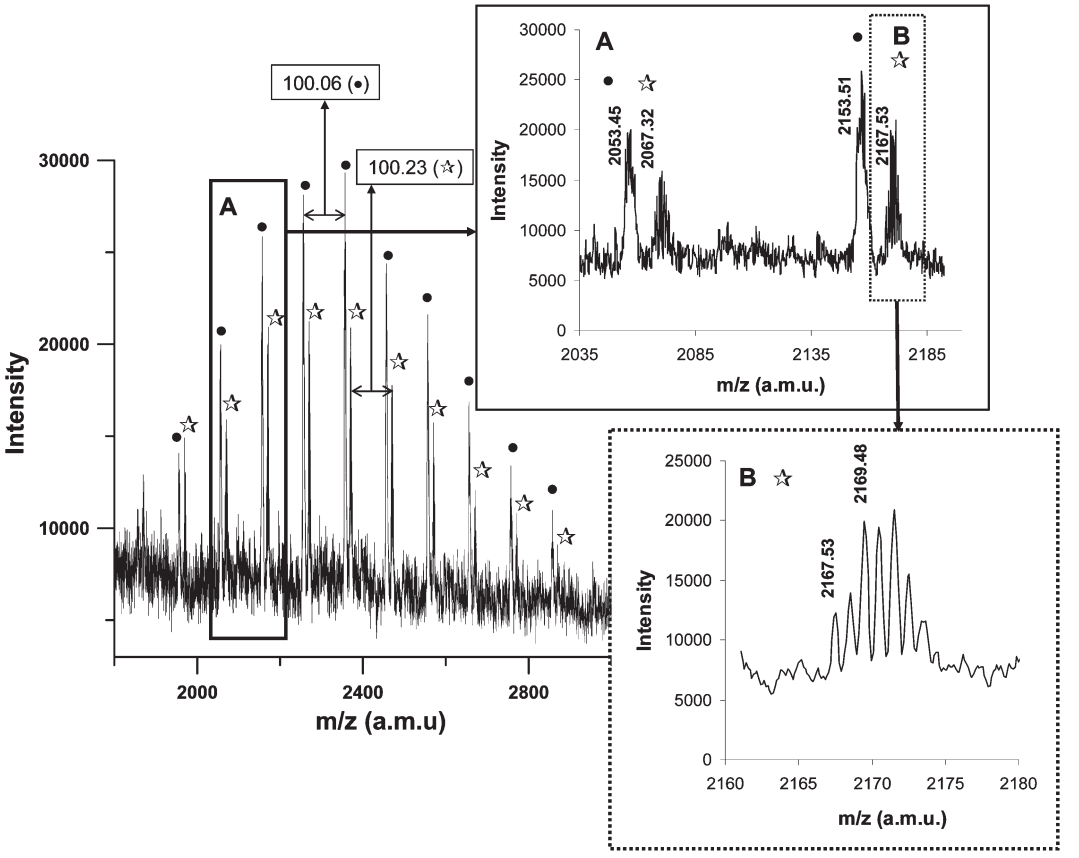

Macromolecular structure and theoretical molar mass of the mono-isotopic peak (g·mol^{-1})

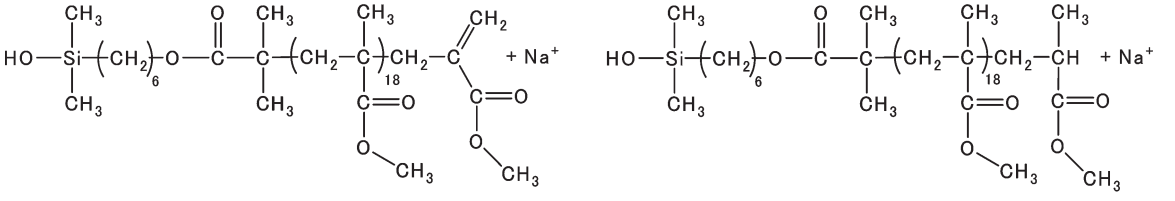

2168.13 **2170.15**

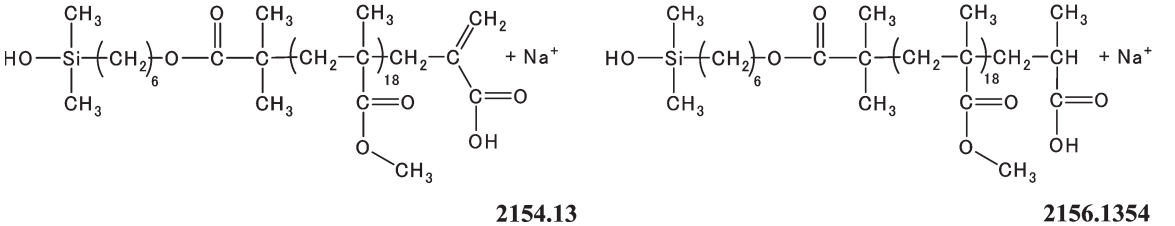

2154.13 **2156.1354**

Figure 6. Analysis of the cleaved PMMA chains after SI−ATRP of MMA initiated from the MSU P123-BiB OMS particles (expt 2 in Table 3): SEC chromatogram and MALDI−TOF mass spectra (reflector mode) of a low M_n fraction recovered after fractionation by semipreparative SEC.

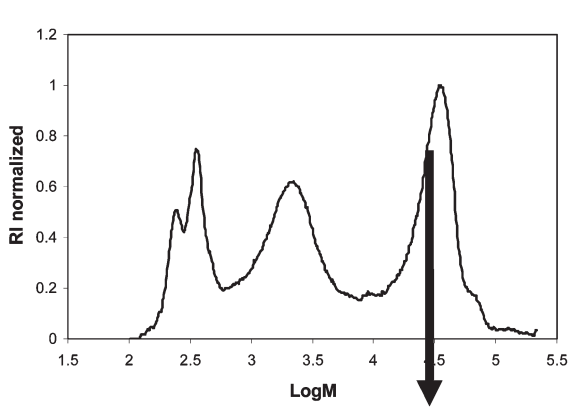

Characteristics of the analyzed PMMA fraction	M_n (g·mol^{-1})	M_w/M_n
SEC	24 190	1.05
MALDI-TOF MS	24 550	1.01

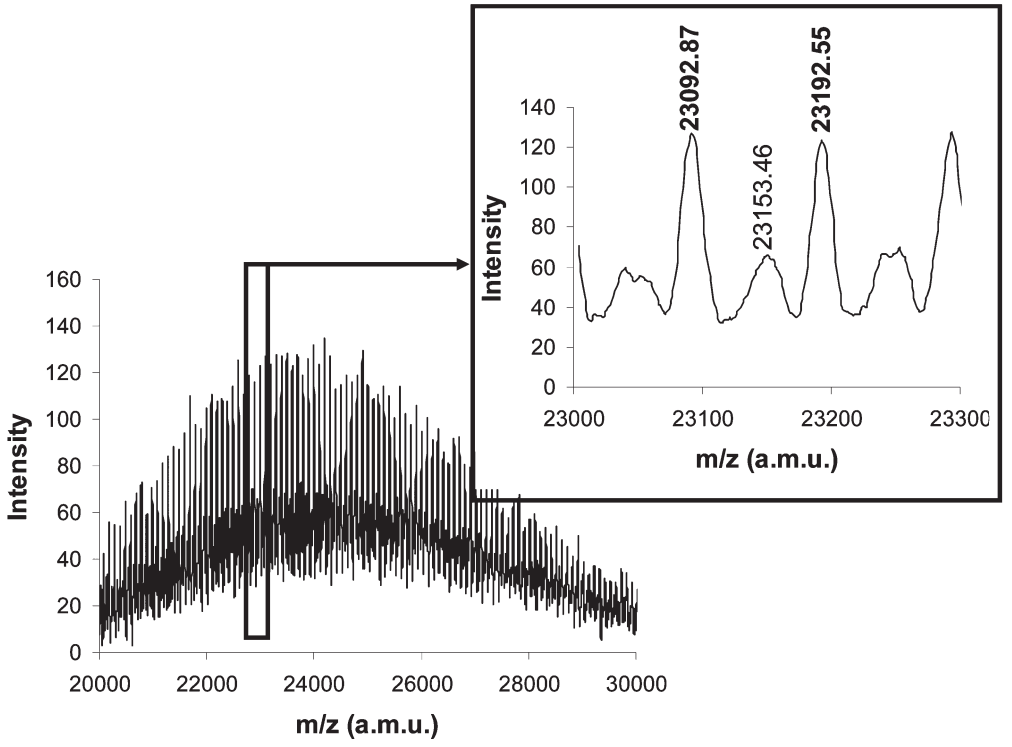

Macromolecular structure and theoretical molar mass of the mono-isotopic peak (g·mol^{-1})

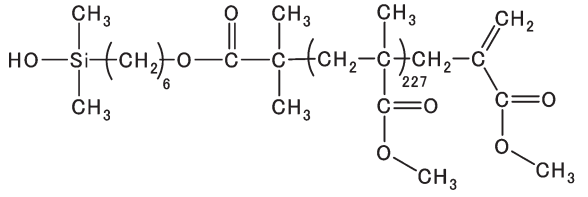

+ Na^+ **23093.7255**

Figure 7. Analysis of the cleaved PMMA chains after SI−ATRP of MMA initiated from the MSU-P123-BP OMS particles (expt 2 in Table 3): MALDI−TOF mass spectra (linear mode) of a high M_n fraction recovered after fractionation by semipreparative SEC.

was then initially introduced in the polymerization medium in combination with the Cu(I) halide activator. All the experimental conditions are reported in Tables 3 and 4 and the results of polymerization are gathered in Table 5, 6 and 7.

As shown in Figure 3, the ATRP of MMA initiated by the free initiator was well-controlled, with a linear increase of the number-average molar masses (M_n) versus monomer conversion together with low polydispersity indexes (PDI < 1.2). The experimental M_n values were above the theoretical ones and we noticed a decrease of the apparent initiator efficiency (f, calculated via the ratio of theoretical M_n over experimental M_n, the theoretical M_n being calculated on the basis of both the free and grafted initiators) when the relative amount of the grafted initiator was increased (Figure 3). This phenomenon was assigned to the low efficiency of the grafted initiator, mainly due to steric hindrance as previously published.[50,51] The evidence of successful grafting of polymer chains was provided by FTIR analysis of the thoroughly washed hybrid particles (Figure SI-4b).

Table 8. Comparison of the PMMA Features of the Hybrid Submicrometeric Particles Synthesized in the Presence of Free Initiator[a]

expt	silica particles	V^b ($cm^3 \cdot g^{-1}$)	$S_{sp}{}^b$ ($m^2 \cdot g^{-1}$)	$D_p{}^b$ (nm)	$S_{sp}/S_{ext}{}^b$	initiator functionalized silica particles	$G_I{}^c$ (BIB·nm^{-2})	PMMA-based hybrid particles	$M_{n,SEC}$ grafted chains/g·mol^{-1} (M_w/M_n)	W $\%_{PMMA}{}^d$
5	SN-1 (Stöber)	0	9	290	1	SN-1-BiB (Stöber)	2.1	SN-1-PMMA	17 890 (1.2)	7
6	CSSN-30 (OMS)	0.16	207	460	28 ± 7	CSSN-30-BiB (OMS)	1.3	CSSN-30-PMMA	43 720 (1.4)	35
7	CSSN-45 (OMS)	0.23	265	380	40 ± 7	CSSN-45-BiB (OMS)	1.2	CSSN-45-PMMA	16 920 (1.4)	23
8	CSSN-105 (OMS)	0.40	560	590	80 ± 7	CSSN-105-BiB (OMS)	1.0	CSSN-105-PMMA	11 675 (2.9)	26
9	MCM-41 (OMS)	0.68	1150	375	72 ± 24	MCM-41-BiB (OMS)	0.4	MCM-41-PMMA	4 000 (6.9)	27

[a] [MMA] = 4.4 ± 0.2 mol·L^{-1}; [DMF] = 0.65 ± 0.15 mol·L^{-1}; [BiB+EBP]:[HMTETA]:[CuCl]:[$CuCl_2$] = 1:1:0.80:0.20; T = 90 °C; MMA: toluene = 50:50 (wt:wt). See further experimental details in Table 3. [b] V = mesopore volume, S_{sp} = specific surface area, D_p = average particle diameter, S_{sp}/S_{ext} = ratio between the specific surface area and the external surface of the particle (see note 58). [c] Initiator grafting density calculated from the overall specific surface area (see eq 1 in the text) [d] Weight amount of grafted PMMA in the hybrid particles: $W\ \%_{PMMA} = W\ \%_{PMMA+initiator+silica} - W\ \%_{initiator+silica}$, with W % the weight loss between 120 and 800 °C obtained from TGA analysis (see Figure SI-11). [e] Bimodal.

SI−ATRP of MMA and S from Micrometric OMS Particles with Large Mesopore Diameters (9−14 nm). The polymerization of MMA and S was performed from the functionalized micrometric OMS particles (MSU-P123, MSU-Brij, and SBA-15) exhibiting ill-defined shape but a perfect arrangement of cylindrical mesopores with different diameters. In contrast to the free chains, the PS and PMMA grafted chains exhibited a multimodal molar mass distribution (Figure 4 and Figure 5, PDI > 3, see expts 2−3 in Table 5, expt 10 in Table 6 and expts 15−17 in Table 7) with a broad peak corresponding to surprisingly short polymer chains and a second peak at high molar masses overlapping with the narrow SEC trace of the free polymer chains.

We investigated the influence of various experimental parameters with the aim of better controlling the polymerization of the grafted chains. Changing the mode of addition of the copper catalyst was ineffective in decreasing the proportion of the low molar mass polymer chains. In order to exclude any influence of the fluoride catalyst used for the synthesis of ordered mesoporous silica particles, we also prepared SBA-15 type OMS particles without fluoride catalyst but at high temperature to avoid microporosity (Table 1).[52] SI−ATRP of MMA was conducted from the functionalized SBA-15-BiB in the presence of free initiator (expt 3 in Table 3). As presented in Figure SI-5, the SEC chromatogram of the cleaved PMMA chains recovered from SBA-15-BiB silica nicely superimposed with the SEC chromatogram of the cleaved PMMA chains from experiment 4 (Table 3, MSU-P123-BiB silica), hence showing the limited role of any residual fluoride catalyst. Moreover, the latter observation underlines the reproducibility of the experimental results concerning the silica etching procedure and the recovery of the cleaved chains.

We then examined the effect of a variation of the ratio of transition metal to ligand for the SI−ATRP of MMA. Indeed, this ratio is a very important parameter influencing the level of control attained in the polymerization as sufficient amount of deactivator catalyst should be present.[53,54] In the case of SI−ATRP from OMS particles, the very high specific surface area might enhance the adsorption of copper species onto the silica surface, inducing a decrease of the local concentration of the efficient copper/ligand complex.[55] The polymerization of MMA initiated from the MSU P123-BiB functionalized OMS particles (mesopore diameter 9.9 nm) was carried out with a default of ligand ([HMTETA]:[Cu] = 0.3:1) and the results were compared with the similar experiment using the quantitative amount of ligand ([HMTETA]:[Cu] = 1:1, expt 2 in Table 3). For both experiments, the molar mass distribution of the free PMMA chains was narrow

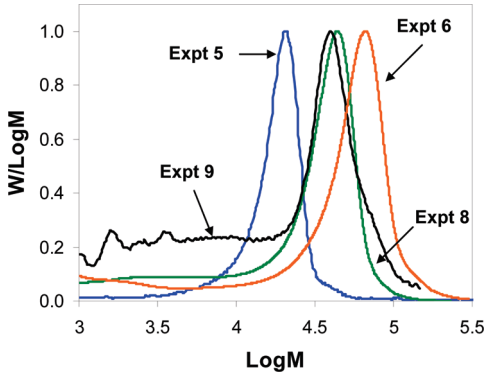

Figure 8. SI−ATRP of MMA from Stöber particles and from core−shell OMS particles with mesopore diameter of 2.5 nm (in the presence of free EBiB initiator): SEC chromatograms of cleaved PMMA chains. See Table 5, expt 5 (SN1-BiB, blue line), expt 6 (CSSN-30-BiB, orange line), expt 8 (CSSN-105-BiB, green line), expt 9 (MCM-41-BiB, black line).

(M_w/M_n < 1.1), which means that the overall concentration of the deactivator was still sufficient to control the polymerization in solution (Figure SI-6). On the other hand, the SEC chromatogram of the grafted chains displayed a bimodal trace with an increased amount of the low molar mass PMMA chains when using a default of ligand (Figure SI-6).

The evolution of both the free and grafted chains was followed as a function of monomer conversion for the ATRP of MMA initiated from MSU P123-BiB particles in the presence of free initiator (Figure 5). As expected, the free PMMA chains were well-controlled with a shift of the SEC chromatograms with conversion and low PDI (Figure 5a). The grafted chains exhibited the already observed bimodal molar mass distribution, in which the high molar mass peak moved with conversion whereas the low molar mass one did not shift with conversion (Figure 5b), suggesting then the presence of both living and dead chains. To further investigate the nature of the grafted polymer chains, fractionation was performed by semipreparative SEC before MALDI−TOF MS analysis of the monodisperse fractions (see Figures 6 and 7).

First, the α-extremity of the cleaved PMMA chains recovered after dissolution of silica with fluorhydric acid is ascribed to a dimethylhydroxysilane group (see Figures 6 and 7). The MALDI−TOF mass spectrum of the low molar mass polymer chains reveals two peak series with a mass difference between the peaks corresponding to the molar mass of the MMA repeat unit, 100.1 g·mol^{-1} (Figure 6). The analysis was recorded in reflector mode and the isotopic distribution of series B depicted in Figure 6 highlighted the

presence of two distinct types of PMMA chains (see details of the theoretical isotopic distributions of PMMA in Figure SI-7). The respective m/z values of the monoisotopic peak and the m/z difference of the two chain structures ($2\ g \cdot mol^{-1}$, see Figure 6, zoom of series B) were consistent with the presence of both aliphatic and unsaturated chain-ends produced by termination reactions via disproportionation. We can notice that the PMMA chains produced by combination reactions were not detected by MALDI−TOF MS analysis. The second peak series A (marked by a dot in Figure 6) is rather ill-defined and might be ascribed to polymer chains with the same chain-end structure as B, in which a methyl ester group has been replaced by a proton (during the cleavage procedure for instance; m/z = 2154.13 amu); or it could be ascribed to ions fragmented in the flight tube and therefore not focalized in the reflector, preventing their structure to be determined.[56] Actually, this second peak series A cannot be assigned to any of the possible structures that may result either from the polymerization or from the cleavage method (Figure SI-8).

The MALDI−TOF mass spectrum of a narrow fraction of the high molar mass PMMA chains is shown in Figure 7 together with the most probable structure and its theoretical molar mass. The molar mass of the main peak series corresponds to PMMA chains containing a dimethylhydroxysilane group at the α-extremity and an unsaturated group at the ω-extremity, each peak of the series being regularly separated by the molar mass of the MMA unit. The absence of peaks corresponding to chains with either a bromine or a chlorine atom at the chain-end is noted whereas it was previously mentioned that the PMMA chains of the high molar mass fraction were living (Figure 5). It is assumed that the unsaturated chain ends were produced by dehydrohalogenation of the living polymer chains during the MALDI−TOF MS analysis.[56]

The MALDI−TOF mass spectra of the cleaved PS chains are reported in Figure SI-9 (low molar mass polymer) and Figure SI-10 (high molar mass polymer). Calculation confirmed the presence of the dimethylhydroxysilane group at the α-end. The mass spectrum of the low molar mass polymer exhibits two peak series corresponding to both saturated and unsaturated chains produced by termination via disproportionation (see comparison with the theoretical isotopic distribution of unsaturated PS chains displayed in ref 56). No peak resulting from termination by combination could be seen. The mass spectrum of the high molar mass polymer was characteristic of chains with unsaturated ω-end group (typical of living polymers having undergone dehydrohalogenation in the source ion).[56] The results are thus in agreement with those found for PMMA.

In conclusion, the combined SEC and MALDI−TOF MS analyses gave us quite a good picture of the structure of the polymer chains grafted from the micrometric OMS particles. They are composed of living macromolecules of high molar mass (in good correlation with the free chains, when present) and of dead chains of low molar mass produced via self-termination of the propagating radicals (only the product of disproportionation was detected). The hypothesis that living chains would be grown from the outer surface only, whereas dead chains would be produced in the confined inner space, is not consistent with the weight proportion of dead vs living chains which is approximately 1:1 as depicted in Figure 5.[57] Nevertheless, the majority of the living chains grafted inside the mesopores might be grown from the surface located near the opening. The shape of the molar mass distribution is thus a direct result of the confined inner space and of the large specific surface area and this particular point is discussed below.

SI−ATRP of MMA from the Submicrometric Spherical OMS Particles (Mesopore Diameters ∼ 2.5 nm). A range of spherical OMS particles (MCM-41 spherical OMS particles and core−shell OMS particles with varying shell thickness (CSSN)) with mesopore diameter of 2.5 nm was synthesized and the TEM pictures are shown in Figure 1. The design of these spherical silica particles with different morphologies was undertaken to provide model substrates exhibiting various ratios of the specific surface area of the mesopores (S_{sp}) over the external surface area of the spherical particle (S_{ext}) (Table 8).[58] To complete the study and allow comparisons, the dense Stöber particles which served as the core template for the elaboration of the core−shell OMS particles were also functionalized with the initiator molecules and used as substrates for similar SI−ATRP experiments.

As reported in Table 8, a decrease of the initiator grafting density with an increase of the specific surface area was noticed. Such an observation might suggest a gradient concentration of the grafted initiator from the outer surface to the inner surface of the mesopores. This is in accordance with previous studies showing that the postsynthesis surface-anchoring of functional molecules into MCM substrates by means of silane coupling agents provides a less uniform distribution of the functional groups throughout the channels in comparison with direct co-condensation synthesis.[59,60] A large proportion of the functional groups can be located inside the channels but near the channel openings.[59] The efficiency of the grafted initiator for the ATRP of MMA was particularly low as shown by the discrepancy between the theoretical and experimental M_n for the grafted chains grown in the absence of free initiator (expts 11−13 in Table 6) or in the presence of 30 mol % of free initiator (expt 6 in Table 5). The comparison between the polymer grafting densities (G_P), reported in Tables 5 and 6, and the initiator grafting densities (G_I) reported in Table 8 confirms the low efficiency of the grafted initiator. From this observation, the occurrence of SI−ATRP from the overall surface of the mesopores may be questionable. However, the discrepancy between the weight amount of PMMA grafted from the spherical OMS particles (> 20 wt %, expts 6−9 in Table 5) and the weight amount of PMMA grafted from the Stöber particles (7 wt %, expt 5 in Table 5) undermines the assumption of polymerization from the sole outer surface. In addition, the large amount of PMMA grafted from the spherical OMS particles in the absence of free initiator (see expts 11−14 in Table 6, $W\%_{PMMA} > 27\%$) undoubtedly showed the presence of polymer inside the 2.5 nm mesopores, as no physisorbed free polymer chains might alter the experimental results.

As reported in Table 8, the PDI of the grafted PMMA chains increased when both the overall mesopore volume and the S_{sp}/S_{ext} ratio were increased. This trend is consistent with the recent results published by Genzer et al.[39] showing the impact of the concave surface of porous substrates with large pores (size of ∼200 nm) on the polydispersity indexes of grafted PMMA (PDI increased from 1.20 for polymer grown in solution to 1.45 for polymer grown inside the pores). Moreover, in contrast to the previous results obtained with micrometric OMS particles, the SEC analyses showed a tailing on the low molar mass side of the main peak but no bimodal shape (Figure 8). Based on the good agreement between M_n of the free chains and M_n of the grafted ones, one can thus conclude that the latter mainly corresponds to living chains. As discussed above, the chains grafted near the

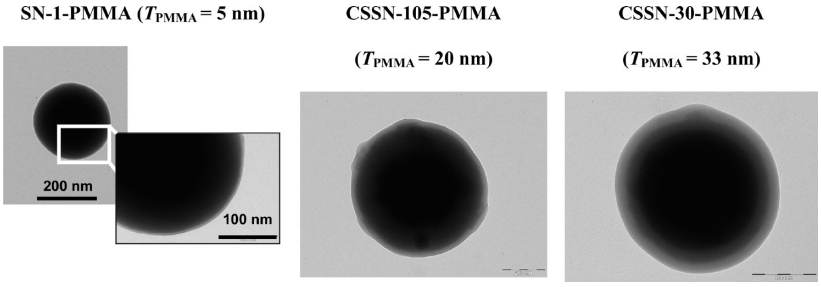

Figure 9. Transmission electron micrographs (TEM) of PMMA-based hybrid particles (see Table 8): Stöber spherical nanoparticles (SN-1-PMMA, expt 5, $M_{n,SEC}$ = 17 890 g·mol^{-1}), core−shell nanoparticles with ordered mesoporous silica shell (CSSN-105-PMMA, expt 8, $M_{n,SEC}$ = 11 675 g·mol^{-1}; CSSN-30-PMMA, expt 6, $M_{n,SEC}$ = 43 720 g·mol^{-1}). T_{PMMA} corresponds to the thickness of the PMMA outer layer. The scale bars corresponds to 200 nm.

pore opening may exhibit a higher degree of livingness in comparison with those located in the inner part.

In conclusion, the fraction of short PMMA dead chains was less pronounced for the well-defined spherical submicrometric OMS particles exhibiting mesopore diameters of 2.5 nm in comparison with the ill-defined micrometric OMS particles formed of mesopores with longer length and diameter of 9−14 nm. Moreover, the SI−ATRP experiments performed from the series of CSSN particles exhibiting similar mesopore diameters but varying mesopore lengths indicated that the molar mass distribution of the grafted chains was affected by the variation of the overall particle size. This suggests that the cylindrical mesopore length induces limitations in the diffusion processes allowing a living polymerization to proceed. Finally, we successfully synthesized multilayered hybrid spherical particles composed of a dense silica core, an inner OMS shell exhibiting varying thicknesses with radial mesopores and a controlled outer PMMA shell grown via surface-initiated ATRP. The TEM pictures of such particles are displayed in Figure 9.

Conclusions

SI−ATRP of methyl methacrylate and styrene was performed from functionalized ordered mesoporous silica (OMS) particles. We synthesized three different kinds of substrates: micrometric OMS particles with ill-defined shape and varying cylindrical mesopore diameters (9−14 nm), submicrometric polydisperse spherical OMS particles and monodisperse core−shell particles composed of a dense silica core and an OMS shell, the latter two particles exhibiting ordered mesopores (diameter 2.5 nm) with radial orientation. By comparing the macromolecular features of the free polymer chains produced in the homogeneous medium by the sacrificial initiator with those of the grafted chains grown from the OMS surface, the present study highlighted an effect of the mesoporous confined space and of the mesoporous channel length on the results of the polymerization. Indeed, a good control of the ATRP of MMA and styrene carried out in the homogeneous medium in the presence of the functionalized OMS particles was observed. On the other hand, the occurrence of irreversible termination reactions inside the mesopores was highlighted by a thorough investigation of the growing polymer chains cleaved from the micrometric OMS particles. Both SEC and MALDI−TOF mass spectrometry analyses proved the presence of dead chains of low molar mass resulting from termination via disproportionation. With a series of submicrometric spherical OMS particles exhibiting mesopore diameters of 2.5 nm and variable mesoporous shell thickness, we showed that of the proportion of short dead chains decreased with a decrease of the average length of the cylindrical mesopores, suggesting an influence of the diffusion processes on the polymerization control. This study not only provides for the first time a mechanistic insight into the SI−ATRP from ordered mesoporous silica of various shapes but also may find applications in material science with the design of structured multilayered hybrid spherical particles composed of an OMS component and a grafted polymer.

Acknowledgment. The authors are grateful to Marie-Odile Sepulchre for her help in polymer fractionation. Joel Belleney is also thanked for the MALDI−TOF MS analyses. French ministry of research, CNRS and ANR (PRISME, Grant No. NT05-3_41901) are gratefully acknowledged for funding. Both laboratories (UMR7610 and UMR7574) were involved in the european FAME network of excellence (FAME*noe*, http://www.famenoe.org/, and EMMI, the European Multifunctional Materials Institute, http://www.emmi-materials.eu/) and the Ph.D. work of H.B. was performed within this framework.

Supporting Information Available: Text giving preparation of the ordered mesoporous silica particles, synthesis of the silylated alkyl bromide initiator, and calculation of the monomer conversion and figures showing plots of X-ray diffraction patterns, FTIR, NMR, SEC/SI−ATRP, and MALDI−TOF MS analyses. This material is available free of charge via the Internet at http://pubs.acs.org.

References and Notes

(1) Wight, A. P.; Davis, M. E. *Chem. Rev.* **2002**, *102*, 3589–3614.
(2) Hunks, W. J.; Ozin, G. A. *J. Mater. Chem.* **2005**, *15*, 3716–3724.
(3) Kresge, C. T.; Leonowicz, M. E.; Roth, W. J.; Vartuli, J. C.; Beck, J. S. *Nature* **1992**, *359*, 710–712.
(4) Hartmann, M. *Chem. Mater.* **2005**, *17*, 4577–4593.
(5) Vallet-Regi, M. *Chem.—Eur. J.* **2006**, *12*, 5934–5943.
(6) Trewyn, B. G.; Giri, S.; Slowing, I. I.; Lin, V. S.-Y. *Chem. Commun.* **2007**, 3236–3245.
(7) Nguyen, T. D.; Liu, Y.; Saha, S.; Leung, K. C.-F.; Stoddart, J. F.; Zink, J. I. *J. Am. Chem. Soc.* **2007**, *129*, 626–634.
(8) Choi, M.; Kleitz, F.; Liu, D.; Lee, H. Y.; Ahn, W.-S.; Ryoo, R. *J. Am. Chem. Soc.* **2005**, *127*, 1924–1932.
(9) Wang, Y.; Caruso, F. *Chem. Mater.* **2005**, *17*, 953–961.
(10) Zhou, Z.; Zhu, S.; Zhang, D. *J. Mater. Chem.* **2007**, *17*, 2428–2433.
(11) Yang, Y.; Yan, X.; Cui, Y.; He, Q.; Li, D.; Wang, A.; Fei, J.; Li, J. *J. Mater. Chem.* **2008**, *18*, 5731–[1] 5737.
(12) Zeng, C.; Han, S.; Yan, X.; Yu, X.; Che, H.; Zhao, X. *Prog. Chem.* **2008**, *20*, 26–32.
(13) Kruk, M.; Dufour, B.; Celer, E. B.; Kowalewski, T.; Jarionec, M.; Matyjaszewski, K. *J. Phys. Chem. B* **2005**, *109*, 9216–9225.
(14) Braunecker, W. A.; Matyjaszewski, K. *Prog. Polym. Sci.* **2007**, *32*, 93–146.
(15) Pyun, J.; Kowalewski, T.; Matyjaszewski, K. *Macromol. Rapid Commun.* **2003**, *24*, 1043–1059.
(16) Yamamoto, S.; Ejaz, M.; Tsujii, Y.; Matsumoto, M.; Fukuda, T. *Macromolecules* **2000**, *33*, 5602–5607.

(17) Yamamoto, S.; Ejaz, M.; Tsujii, Y.; Fukuda, T. *Macromolecules* **2000**, *33*, 5608–5612.
(18) Hawker, C. J.; Bosman, A. W.; Harth, E. *Chem. Rev.* **2001**, *101*, 3661–3688.
(19) Matyaszewski, K.; Xia, J. *Chem. Rev.* **2001**, *101*, 2921–2990.
(20) Kamigaito, M.; Ando, T.; Sawamoto, M. *Chem. Rev.* **2001**, *101*, 3689–3745.
(21) Chong, Y. K.; Krstina, J.; Le, T. P. T.; Moad, G.; Postma, A.; Rizzardo, E.; Thang, S. H. *Macromolecules* **2003**, *36*, 2256–2272.
(22) Pyun, J.; Matyjaszewski, K. *Chem. Mater.* **2001**, *13*, 3436–3448.
(23) *Polymer Brushes*; Advincula, R. C., Brittain, W. J., Caster, K. C., Ruhe, J., Eds; Wiley-VCH: Weinheim, Germany, 2004.
(24) Radhakrishnan, B.; Ranjan, R.; Brittain, W. J. *Soft Matter* **2006**, *2*, 386–396.
(25) Tsujii, Y.; Ohno, K.; Yamamoto, S.; Goto, A.; Fukuda, T. *Adv. Polym. Sci.* **2006**, *197*, 1–45.
(26) Ghannam, L.; Parvole, J.; Laruelle, G.; Francois, J.; Billon, L. *Polym. Int.* **2006**, *55*, 1199–1207.
(27) Zou, H.; Wu, S.; Shen, J. *Chem. Rev.* **2008**, *108*, 3893–3957.
(28) Ohno, K.; Morinaga, T.; Koh, K.; Tsujii, Y.; Fukuda, T. *Macromolecules* **2005**, *38*, 2137–2142.
(29) Bartholome, C.; Beyou, E.; Bourgeat-Lami, E.; Chaumont, P.; Zydowicz, N. *Macromolecules* **2003**, *36*, 7946–7952.
(30) Parvole, J.; Laruelle, G.; Khoukh, A.; Billon, L. *Macromol. Chem. Phys.* **2005**, *206*, 372–382.
(31) Fischer, H. *Chem. Rev.* **2001**, *101*, 3581–3610.
(32) Moreno, J.; Sherrington, D. C. *Chem. Mater.* **2008**, *20*, 4468–4474.
(33) Fu, Q.; Rama Rao, G. V.; Ista, L. K.; Wu, Y.; Andrzejewski, B. P.; Sklar, L. A.; Ward, T. L.; Lopez, G. P. *Adv. Mater.* **2003**, *15*, 1262–1266.
(34) Save, M.; Granvorka, G.; Bernard, J.; Charleux, B.; Boissière, C.; Grosso, D.; Sanchez, C. *Macromol. Rapid Commun.* **2006**, *27*, 393–398.
(35) Audouin, F.; Blas, H.; Pasetto, P.; Beaunier, P.; Boissiere, C.; Sanchez, C.; Save, M.; Charleux, B. *Macromol. Rapid Commun.* **2008**, *29*, 914–921.
(36) Lenarda, M.; Chessa, G.; Moretti, E.; Polizzi, S.; Storaro, L.; Talon, A. *J. Mater. Sci.* **2006**, *41*, 6305–6312.
(37) Hong, C. Y.; Li, X.; Pan, C.-Y. *Eur. Polym. J.* **2007**, *43*, 4114–4122.
(38) Kruk, M.; Dufour, B.; Celer, E. B.; Kowalewski, T.; Jaroniec, M.; Matyjaszewski, K. *Macromolecules* **2008**, *41*, 8584–8591.
(39) Gorman, C. B.; Petrie, R. J.; Genzer, J. *Macromolecules* **2008**, *41*, 4856–4865.
(40) Uemura, T.; Ono, Y.; Kitagawa, K.; Kitagawa, S. *Macromolecules* **2008**, *41*, 87–94.
(41) Boissière, C.; Larbot, A.; van der Lee, A.; Kooyman, P. J.; Prouzet, E. *Chem. Mater.* **2000**, *12*, 2902–2913.
(42) Zhao, D.; Feng, J.; Huo, Q.; Melosh, N.; Fredrickson, G. H.; Chmelka, B. F.; Stucky, G. D. *Science* **1998**, *279*, 548–552.
(43) Kresge, C. T.; Leonowicz, M. E.; Roth, W. J.; Vartuli, J. C.; Beck, J. S. *Nature* **1992**, *359*, 710–712.
(44) Yoon, S. B.; Kim, J.-Y.; Kim, J. H.; Park, Y. J.; Yoon, K. R.; Park, S.-K.; Yu, J.-S. *J. Mater. Chem.* **2007**, *17*, 1758–1761.
(45) Li, C.; Benicewicz, B. C. *Macromolecules* **2005**, *38*, 5929–5936.
(46) Prouzet, E.; Cot, F.; Nabias, G.; Larbot, A.; Kooyman, P.; Pinnavaia, T. J. *Chem. Mater.* **1999**, *11*, 1498–1503.
(47) Carrot, G.; Diamanti, S.; Manuszak, M.; Charleux, B.; Vairon, J.-P. *J. Polym. Sci. Part A, Polym. Chem.* **2001**, *39*, 4294–4301.
(48) Pyun, J.; Jia, S.; Kowalewski, T.; Patterson, G. D.; Matyjaszewski, K. *Macromolecules* **2003**, *36*, 5094–5104.
(49) Matyjaszewski, K.; Miller, P. J.; Shukla, N.; Immaraporn, B.; Gelman, A.; Luokala, B. B.; Siclovan, T. M.; Kickelbick, G.; Vallant, T.; Hoffmann, H.; Pakula, T. *Macromolecules* **1999**, *32*, 8716–8724.
(50) Bartholome, C.; Beyou, E.; Bourgeat-Lami, E.; Chaumont, P.; Zydowicz, N. *Macromolecules* **2003**, *36*, 7946–7952.
(51) Ohno, K.; Morinaga, T.; Koh, K.; Tsujii, Y.; Fukuda, T. *Macromolecules* **2005**, *38*, 2137–2142.
(52) Zhao, D.; Feng, J.; Huo, Q.; Melosh, N.; Frederickson, G. H.; Chmelka, B. F.; Stucky, G. D. *Science* **1998**, *279*, 548–552.
(53) Nanda, A. K.; Matyjaszewski, K. *Macromolecules* **2003**, *36*, 1487–1493.
(54) Huang, J.; Pintauer, T.; Matyjaszewski *J. Polym. Sci.: Part A, Polym. Chem.* **2004**, *42*, 3285–3292.
(55) Nguyen, J. V.; Jones, C. W. *J. Polym. Sci: Part A: Polym. Chem.* **2004**, *42*, 1367–1383.
(56) Ladavière, C.; Lacroix-Desmazes, P.; Delolme, F. *Macromolecules* **2008**, *42*, 70–84.
(57) Considering that the total amount of PMMA from TGA is 30% (weight loss is 50%: 20% for the initiator and 30% for the polymer) and that the external surface area is in the $1-2\ m^2\cdot g^{-1}$ range, 0.5 g of silica displays $1 \times 10^{18}\ nm^2$ of maximum external surface grafted with 0.3 g of PMMA. If we consider that only 50 wt % of the chains are grafted from the external surface (i.e., the living chains which represent 50% of the total mass on the SEC chromatogram, Figure 5), then the mass of grafted PMMA is 0.15 g. On the basis of $M_n = 34\,040\ g\cdot mol^{-1}$, the calculated grafting density of the polymer is 2.6 chains$\cdot nm^{-2}$, which is far above the classical experimental value of 0.5 chains$\cdot nm^{-2}$ for stretched polymer brushes.
(58) The external surface area of one particle was calculated as follows: $S_{ext} = 4\pi(D_p/2)^2$, with D_p the diameter of the spherical particle. The specific surface area of the mesopores forming the OMS shell was calculated as follows: $Ssp = (V_p - V_{core}) \times \rho_{OMS} \times S_{sp,\ MCM\text{-}41}$, with ρ_{OMS} the density of ordered mesoporous silica ($\rho_{OMS} \sim 1.0\ g.cm^{-3}$), V_p the volume of the particle, V_{core} the volume of the nonporous core and $S_{sp,\ MCM\text{-}41}$ the specific surface area of the entirely mesoporous spherical particles (MCM-41, see Table 1): S_{sp}, MCM-41 $= 1150\ m^2\cdot g^{-1}$.
(59) Stein, A.; Melde, B. J.; Schroden, R. C. *Adv. Mater.* **2000**, *12*, 1403–1419.
(60) Kecht, J.; Schlossbauer, A.; Bein, T. *Chem. Mater.* **2008**, *20*, 7207–7214.